A No-Reconstruction Fault-Tolerant Control Method for Open-Switch Faults in Standard IM Drives

Lei WANG, Yingying SHE, Yujin SONG, Weikang WANG, and Zhixi WU

Abstract—**The power switch faults in standard two-level three-phase inverter-fed motor drives cause severe speed oscillation, and decline the system stability. The fault-tolerant methods which require topology reconstruction have the disadvantages of additional cost and unreliability. It is of great significance to study the no-reconstruction fault-tolerant (NFT) method, which only changes the control algorithm. In this paper, a novel NFT method is proposed for induction motor (IM) drive, which consists of the two-mode control algorithm and the algorithm transition strategy. In the healthy mode, conventional model predictive flux control (MPFC) is adopted; in the tolerant mode, a novel MPFC algorithm is proposed to eliminate the effect of the fault power switch by setting the reference fault phase current as zero. The two modes alternate in each current cycle. An algorithm transition strategy is proposed for the smooth transition of two modes, which has the ability to revert to healthy operation even if misdiagnoses occur. The proposed NFT method can significantly reduce the speed oscillation after the fault occurs, and experiment results verify its effectiveness.**

Index Terms—**Algorithm transition strategy, no-reconstruction fault-tolerant method, standard induction motor drive, two-mode model predictive flux control algorithm.**

I. Introduction

TWO-LEVEL three-phase inverter-fed motor drives are most widely used in many industrial occasions due to their simple structure and low cost. However, the reliability of the two-level three-phase inverter is not enough because of the topology limitation. The inverter faults, which can be divided into short-switch and open-switch faults, account for a large percentage of motor drive faults [1]. The short-switch faults are usually converted to open-switch faults by hardware protection [2]. The open-switch faults cause the loss of inverter voltage vector, leading to severe speed oscillation or even the motor drive shutdown.

With the increasing demand for high reliability, the research on inverter fault tolerance is of great significance. Researchers have proposed some more complex topologies to improve the inverter fault-tolerant ability, such as four-leg inverter [3], [4], dual inverter [5], [6], and multilevel inverter [7], [8]. This scheme aims to increase the number of voltage vectors so that the motor drive can still operate after missing part of the voltage vector, called the passive fault tolerance (PFT). However, the cost of these topologies is greatly higher than standard motor drives. In recent years, the fault-tolerant methods of the standard motor drive have attracted more and more attention, whose idea is to adjust inverter topology and control algorithm after the fault diagnosis, called the active fault tolerance (AFT). Fault diagnosis can detect and locate the fault switch, whose scheme generally includes data processing, feature extraction, and fault classification [9], [10]. It is the precondition of AFT.

The most simple AFT method is to add redundant legs or inverters. After fault diagnosis, the fault leg or inverter is replaced by a redundant one. Further, switch-reduced fault-tolerant methods have been proposed to avoid the cost of redundant legs or inverters, such as four-switch inverter [11]–[13], four-switch four leg inverter [14], mono-inverter dual motor drive [15]–[17], four-leg inverter dual motor drive [18], [19], and five-leg inverter dual motor drive [20], [21]. After fault diagnosis, the fault leg is isolated, and the inverter topology turns to the suitable tolerant topologies by certain switches. Generally, the motor phase terminal or the neutral point is reconnected to the capacitor mid-point or healthy leg. Although the AFT can save high costs compared to PFT, it still has many disadvantages: it needs lots of redundant switches to realize the topology reconstruction; the other healthy power switch in the isolated leg is wasted; designing suitable fault-tolerant topologies and control methods for different fault situations is also a big challenge.

Hence, realizing the fault tolerance of standard motor drives without topology reconstruction is of great meaning, called the no-reconstruction fault tolerance (NFT). The NFT method only changes the control algorithm after fault diagnosis at no extra cost. Researchers have realized NFT for open-phase faults of PMSM drive based on finite control set model predictive control [22], [23]. A fault-tolerant current control method has been proposed for open-switch faults of permanent-magnet generator system [24]. However, these methods ignore the healthy power switch in the fault leg, causing big torque loss. To fully utilize the remaining healthy power switches in standard PMSM drive, research in [25] has proposed a current optimization-based NFT method for open-switch and open-phase faults, and research in [26] has proposed a field-oriented

Manuscript received June 13, 2025; revised September 1, 2025; accepted October 10, 2025. Date of publication December 30, 2025; date of current version December 2, 2025. No funding was received to assist with the preparation of this manuscript.(*Corresponding author: Yujin Song.*)

All authors are with the Wuhan Second Ship Design and Research Institute, Wuhan 430200, China (e-mail: 15809705@qq.com; 1072608260@qq.com; wy_syj960110@163.com; hhwangweikang@foxmail.com; 15827276876@163.com).

Digital Object Identifier 10.24295/CPSSTPEA.2025.00036

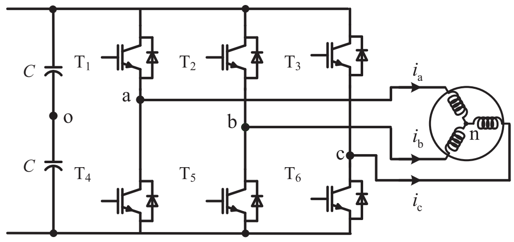

Fig. 1. The circuit diagram of standard IM drive.

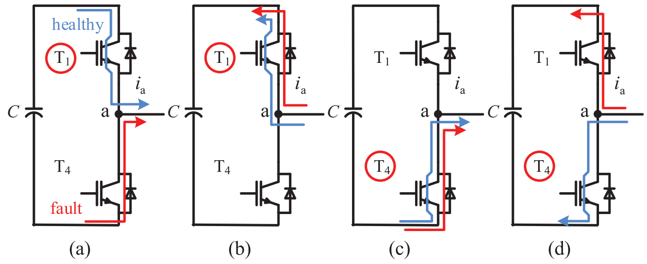

Fig. 2. The current circuits of inverter leg a. (a) $S_a = 1$, $i_a > 0$, (b) $S_a = 1$, $i_a < 0$, (c) $S_a = 0$, $i_a > 0$, (d) $S_a = 0$, $i_a < 0$.

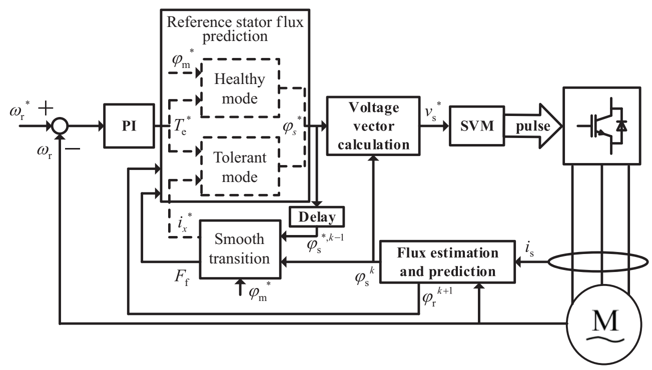

Fig. 3. The control diagram of proposed NFT method.

control-based NFT method to improve the current tracking and algorithm transition for open-switch faults. In these methods, the five healthy power switches are all used in fault tolerance. Thus, the system can work in the healthy state for half of each current cycle and in the tolerant state for the other half, obtaining a better control performance. However, both researches directly control the currents in the two-phase rotating coordinate system. It means that electrical angle estimation is unavoidable, whose accuracy can affect the reference tracking and the control algorithm transition. Besides, the fault type is considered known, meaning additional fault diagnosis is required in practice.

In this paper, a model predictive flux control (MPFC)-based NFT method for standard induction motor (IM) drive is proposed, where the five healthy power switches are all used in fault tolerance. The contributions can be listed as follows:

1. The proposed two-mode control algorithm directly controls the stator flux vector in the static coordinate system, avoiding the requirement of static-to-rotating coordinate transformation and electrical angle estimation. It is general for any switch faults.

2. The proposed algorithm transition strategy can realize not only the fast fault diagnosis but also the smooth control algorithm transition. Especially, it has the ability to revert to healthy operation even if misdiagnoses occur.

This paper is organized as follows. The proposed two-mode control algorithm is presented in Section II, and the algorithm transition strategy is discussed in Section III. Then, Section IV shows the experiment results, and Section V gives the conclusion.

II. Proposed Two-Mode Control Algorithm

The topology of the standard IM drive is shown in Fig. 1. C is the DC bus capacitor. a, b, c are three inverter legs. o is the capacitor mid-point. n is the motor neutral point. i_a, i_b, i_c are phase currents. T_x ($x = 1 - 6$) are six power switches. Each inverter leg has two switching states S_x (x = a, b, c), where '1' means upper switch on, and '0' means lower switch on.

A. IM Model

The model of IM in the static coordinate system can be expressed as

$$\boldsymbol{x} = \boldsymbol{A}\boldsymbol{x} + \boldsymbol{B}\boldsymbol{v}_s \tag{1}$$

where $\boldsymbol{A} = \begin{bmatrix} -\lambda(R_sL_r + R_rL_s) + j\omega_r & \lambda(R_r - jL_r\omega_r) \\ -R_s & 0 \end{bmatrix}$, $\lambda = 1/(L_sL_r - L_m^2)$, $\boldsymbol{x} = [\boldsymbol{i}_s \quad \boldsymbol{\varphi}_s]^T$, $\boldsymbol{B} = [\lambda L_r \quad 1]^T$, $\boldsymbol{i}_s$, $\boldsymbol{\varphi}_s$, and $\boldsymbol{v}_s$ are stator current, stator flux, and voltage vectors, respectively. L_m, L_s, and L_r are mutual, stator, and rotor inductance, R_s and R_r are stator and rotor resistance, ω_r is electrical rotor speed.

The output torque T_e can be calculated as

$$T_e = 1.5 n_p \lambda L_m (\boldsymbol{\varphi}_r \otimes \boldsymbol{\varphi}_s) \tag{2}$$

where n_p is the number of pole pairs, $\otimes$ means cross-product operation, $\boldsymbol{\varphi}_r$ is the rotor flux vector.

B. Control Basic

Inverter leg a as an example, the current circuits under different switching states are shown in Fig. 2. It shows that the T_1 fault doesn't affect the control of IM drive when i_a is negative, and the T_4 fault doesn't affect the control of IM drive when i_a is positive. Thus, after a power switch fault occurs, the current cycle of the fault leg can be divided into two parts: healthy and fault parts. In the fault part, the control algorithm must be adjusted for fault tolerance.

The control diagram of the proposed NFT method is shown in Fig. 3. First, the reference torque is obtained by Proportional-Integral (PI) regulator. Then, the inverter voltage vector is directly calculated by the proposed two-mode control algorithm, which consists of the control algorithms in healthy and tolerant modes. Here, the stator flux vector is used for the smooth algorithm transition. Last, the control signals of power switches are generated by space vector pulse width modulation (SVM).

C. Control Algorithm of Healthy Mode

The predictive model of (1) can be derived by Euler-forward method as

$$\boldsymbol{x}^{k+1} = (1 + \boldsymbol{A}T_{\mathrm{s}})\,\boldsymbol{x}^{k} + \boldsymbol{B}T_{\mathrm{s}}\boldsymbol{v}_{\mathrm{s}}^{k} \tag{3}$$

where T_{s} is sampling period. The superscript k means the value at the step k.

According to (2), the output torque at step k+1 can be predicted as

$$T_{\mathrm{e}}^{k+1} = 1.5n_{\mathrm{p}}\lambda L_{\mathrm{m}}\,(\boldsymbol{\varphi}_{\mathrm{r}}^{k+1} \otimes \boldsymbol{\varphi}_{\mathrm{s}}^{k+1}) \tag{4}$$

Substituting T_{e}^{k+1} and $\boldsymbol{\varphi}_{\mathrm{s}}^{k+1}$ by their reference values, the predictive model of (2) can be expressed by

$$T_{\mathrm{e}}^{*} = 1.5n_{\mathrm{p}}\,\lambda L_{\mathrm{m}}\,(\boldsymbol{\varphi}_{\mathrm{r}}^{k+1} \otimes \boldsymbol{\varphi}_{\mathrm{s}}^{*}) \tag{5}$$

The rotor flux at step k+1 can be predicted by

$$\boldsymbol{\varphi}_{\mathrm{r}}^{k+1} = \boldsymbol{\varphi}_{\mathrm{r}}^{k} + T_{\mathrm{s}}\,(\frac{R_{\mathrm{r}}L_{m}}{L_{\mathrm{r}}}\,\boldsymbol{i}_{\mathrm{s}}^{k} - (\frac{R_{\mathrm{r}}}{L_{\mathrm{r}}} - \mathrm{j}\omega_{\mathrm{r}})\,\boldsymbol{\varphi}_{\mathrm{r}}^{k}) \tag{6}$$

Taking $\boldsymbol{\varphi}_{\mathrm{r}}^{k+1}$ as known, the reference stator flux can be calculated by (5)

$$\begin{gathered}\boldsymbol{\varphi}_{\mathrm{s}}^{*} = \boldsymbol{\varphi}_{\mathrm{m}}^{*}\cdot \exp(\,\mathrm{j}\angle\,\boldsymbol{\varphi}_{\mathrm{s}}^{*}),\ \angle\,\boldsymbol{\varphi}_{\mathrm{s}}^{*} = \angle\,\boldsymbol{\varphi}_{\mathrm{r}}^{k+1} + \theta^{k+1}\\ \theta^{k+1} = \arcsin\left(\frac{T_{\mathrm{e}}^{*}}{1.5n_{\mathrm{p}}\lambda L_{\mathrm{m}}|\boldsymbol{\varphi}_{\mathrm{r}}^{k+1}|\boldsymbol{\varphi}_{\mathrm{m}}^{*}}\right)\end{gathered} \tag{7}$$

where $\boldsymbol{\varphi}_{\mathrm{m}}^{*}$ is the reference value of stator flux amplitude, θ^{k+1} is the angle difference of $\boldsymbol{\varphi}_{\mathrm{s}}^{*}$ and $\boldsymbol{\varphi}_{\mathrm{r}}^{k+1}$.

According to (3), the stator flux at step k+1 can be predicted as

$$\boldsymbol{\varphi}_{\mathrm{s}}^{k+1} = (\boldsymbol{v}_{\mathrm{s}} - R_{\mathrm{s}}\boldsymbol{i}_{\mathrm{s}}^{k})T_{\mathrm{s}} + \boldsymbol{\varphi}_{\mathrm{s}}^{k} \tag{8}$$

Substituting $\boldsymbol{\varphi}_{\mathrm{s}}^{k+1}$ and $\boldsymbol{v}_{\mathrm{s}}$ by their reference values, the reference voltage vector can be calculated as

$$\boldsymbol{v}_{\mathrm{s}}^{*} = \frac{\boldsymbol{\varphi}_{\mathrm{s}}^{*} - \boldsymbol{\varphi}_{\mathrm{s}}^{k}}{T_{\mathrm{s}}} + R_{\mathrm{s}}\,\boldsymbol{i}_{\mathrm{s}}^{k} \tag{9}$$

D. Control Algorithm of Tolerant Mode

When IM operates in the fault part, the current circuit is changed as Fig. 2 shows. It makes the actual and reference inverter vectors different. Since the fault leg current in the fault part can be approximated to zero, T_{e} and $|\,\boldsymbol{\varphi}_{\mathrm{s}}\,|$ can't be constant simultaneously.

Hence, in the proposed algorithm, the $|\,\boldsymbol{\varphi}_{\mathrm{s}}\,|$ is no longer controlled constantly. Instead, the reference fault leg current is set to zero under tolerant mode to eliminate the effect of fault switch.

According to (3), the relationship between $\boldsymbol{i}_{\mathrm{s}}^{k+1}$ and $\boldsymbol{\varphi}_{\mathrm{s}}^{k+1}$ can be rewrote as

$$\boldsymbol{i}_{\mathrm{s}}^{k+1} = \left(1 + \frac{T_{\mathrm{s}}}{\tau_{\sigma}}\right)\boldsymbol{i}_{\mathrm{s}}^{k} + \frac{T_{\mathrm{s}}}{(T_{\mathrm{s}} + \tau_{\sigma})R_{\sigma}}\cdot \left(\left(\frac{k_{\mathrm{r}}}{(\tau_{\mathrm{r}})} - \mathrm{j}\omega_{\mathrm{r}}k_{\mathrm{r}}\right)\boldsymbol{\psi}_{\mathrm{r}}^{k} + \frac{\boldsymbol{\varphi}_{\mathrm{s}}^{k+1} - \boldsymbol{\varphi}_{\mathrm{s}}^{k}}{T_{\mathrm{s}}} + R_{\mathrm{s}}\boldsymbol{i}_{\mathrm{s}}^{k}\right) \tag{10}$$

where $k_{\mathrm{r}} = L_{\mathrm{m}}/L_{\mathrm{r}}$, $R_{\sigma} = R_{\mathrm{s}} + k_{\mathrm{r}}^{2}R_{\mathrm{r}}$, $\tau_{\sigma} = 1/(\lambda L_{\mathrm{r}}R_{\sigma})$, $\tau_{\mathrm{r}} = L_{\mathrm{r}}/R_{\mathrm{r}}$.

Substituting $\boldsymbol{i}_{\mathrm{s}}^{k+1}$ and $\boldsymbol{\varphi}_{\mathrm{s}}^{k+1}$ by their reference values in (10), the components of $\boldsymbol{\varphi}_{\mathrm{s}}^{*}$ in the two-phase static coordinate system can be calculated as

$$\begin{bmatrix}\boldsymbol{\varphi}_{\mathrm{s}\alpha}^{*}\\ \boldsymbol{\varphi}_{\mathrm{s}\beta}^{*}\end{bmatrix} = (T_{\mathrm{s}} + \tau_{\sigma})R_{\sigma}\begin{bmatrix}\boldsymbol{i}_{\mathrm{s}\alpha}^{*}\\ \boldsymbol{i}_{\mathrm{s}\beta}^{*}\end{bmatrix} = \begin{bmatrix}M\\ N\end{bmatrix} \tag{11}$$

where $M = \boldsymbol{\varphi}_{\mathrm{s}\alpha}^{k}R_{\sigma}(T_{\mathrm{s}} + \tau_{\sigma})^{2}/\tau_{\sigma}\boldsymbol{i}_{\alpha}^{k} - (k_{\mathrm{r}}/\tau_{\mathrm{r}}\boldsymbol{\varphi}_{\mathrm{r}\alpha}^{k} + \omega_{\mathrm{r}}k_{\mathrm{r}}\boldsymbol{\varphi}_{\mathrm{r}\beta}^{k} + R_{\mathrm{s}}\boldsymbol{i}_{\alpha}^{k})T_{\mathrm{s}}$, $N = \boldsymbol{\varphi}_{\mathrm{s}\beta}^{k} - R_{\sigma}(T_{\mathrm{s}} + \tau_{\sigma})^{2}/\tau_{\sigma}\boldsymbol{i}_{\beta}^{k} - (k_{\mathrm{r}}/\tau_{\mathrm{r}}\boldsymbol{\varphi}_{\mathrm{r}\beta}^{k} - \omega_{\mathrm{r}}k_{\mathrm{r}}\boldsymbol{\varphi}_{\mathrm{r}\alpha}^{k} + R_{\mathrm{s}}\boldsymbol{i}_{\beta}^{k})T_{\mathrm{s}}$. The subscripts α, β mean the components of variables in the two-phase static coordinate system.

The components of $\boldsymbol{\varphi}^{*}$ in the three-phase static coordinate system can be represented as

$$\begin{bmatrix}\boldsymbol{\varphi}_{\mathrm{sa}}^{*}\\ \boldsymbol{\varphi}_{\mathrm{sb}}^{*}\\ \boldsymbol{\varphi}_{\mathrm{sc}}^{*}\end{bmatrix} = (T_{\mathrm{s}} + \tau_{\sigma})R_{\sigma}\begin{bmatrix}\boldsymbol{i}_{\mathrm{sa}}^{*}\\ \boldsymbol{i}_{\mathrm{sb}}^{*}\\ \boldsymbol{i}_{\mathrm{sc}}^{*}\end{bmatrix} + \begin{bmatrix}1 & 0\\ -\frac{1}{2} & \frac{\sqrt{3}}{2}\\ -\frac{1}{2} & -\frac{\sqrt{3}}{2}\end{bmatrix}\begin{bmatrix}M\\ N\end{bmatrix} \tag{12}$$

where the subscripts a, b, c mean the components of variables in the three-phase static coordinate system.

Once the reference fault leg current is set to zero, the corresponding component of $\boldsymbol{\varphi}_{\mathrm{s}}^{*}$ can be obtained. For example, if i_{sa}^{*} is set zero, $\boldsymbol{\varphi}_{\mathrm{sa}}^{*}$ can be calculated by (12). Substituting $\boldsymbol{\varphi}_{\mathrm{sa}}^{*}$ into (5), the other components of $\boldsymbol{\varphi}_{\mathrm{s}}^{*}$ can be finally obtained. The cases of leg b and c are similar.

Then, the reference stator flux in the two-phase static coordinate system can be calculated as

$$\begin{bmatrix}\boldsymbol{\varphi}_{\mathrm{s}\alpha}^{*}\\ \boldsymbol{\varphi}_{\mathrm{s}\beta}^{*}\end{bmatrix} = \begin{cases}\begin{bmatrix}\boldsymbol{\varphi}_{\mathrm{s}\alpha}^{*}\\ \dfrac{T_{\mathrm{e}}^{*}/(1.5n_{\mathrm{p}}\lambda L_{\mathrm{m}}) + \boldsymbol{\varphi}_{\mathrm{s}\alpha}^{*}\boldsymbol{\varphi}_{\mathrm{r}\beta}^{k+1}}{\boldsymbol{\varphi}_{\mathrm{r}\alpha}^{\mathrm{k+1}}}\end{bmatrix}, & if\ \boldsymbol{i}_{\mathrm{sa}}^{*} = 0\\ \begin{bmatrix}\dfrac{\sqrt{3}\,T_{\mathrm{e}}^{*}/(\boldsymbol{\varphi}_{\mathrm{r}\alpha}^{k+1}1.5n_{\mathrm{p}}\lambda L_{\mathrm{m}}) - 2\boldsymbol{\varphi}_{\mathrm{sb}}^{*}}{1 - \sqrt{3}\,\boldsymbol{\varphi}_{\mathrm{r}\beta}^{k+1}/\boldsymbol{\varphi}_{\mathrm{r}\alpha}^{k+1}}\\ (\boldsymbol{\varphi}_{\mathrm{s}\alpha}^{*} + 2\boldsymbol{\varphi}_{\mathrm{sb}}^{*})\sqrt{3}\end{bmatrix}, & if\ \boldsymbol{i}_{\mathrm{sb}}^{*} = 0\\ \begin{bmatrix}\dfrac{\sqrt{3}\,T_{\mathrm{e}}^{*}/(\boldsymbol{\varphi}_{\mathrm{r}\alpha}^{k+1}1.5n_{\mathrm{p}}\lambda L_{\mathrm{m}}) + 2\boldsymbol{\varphi}_{\mathrm{sc}}^{*}}{-\sqrt{3}\,\boldsymbol{\varphi}_{\mathrm{r}\beta}^{k+1}/\boldsymbol{\varphi}_{\mathrm{r}\alpha}^{k+1}}\\ -(\boldsymbol{\varphi}_{\mathrm{s}\alpha}^{*} + 2\boldsymbol{\varphi}_{\mathrm{sb}}^{*})/\sqrt{3}\end{bmatrix}, & if\ \boldsymbol{i}_{\mathrm{sc}}^{*} = 0\end{cases} \tag{13}$$

Substituting (13) into (9), the reference voltage vector under tolerant mode can be obtained.

E. Phase Current Protection

According to the above analysis, the control logic of the proposed algorithm is to maintain the phase current of the fault leg as zero by controlling the corresponding phase component of $\boldsymbol{\varphi}_{\mathrm{s}}^{*}$ in the three-phase static coordinate system. And the reference torque is generated by the other healthy phases. However, when the denominator in (13) is near zero, the calculated healthy phase components of $\boldsymbol{\varphi}_{\mathrm{s}}^{*}$ will be too large. As (10) shows, the healthy phase currents will also come to a high

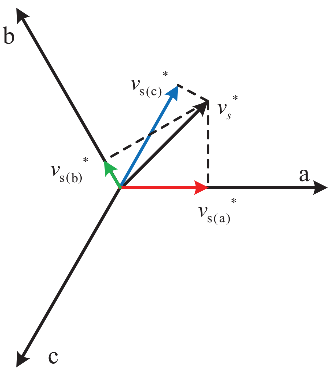

Fig. 4. The adjusted reference voltage vector for phase current protection.

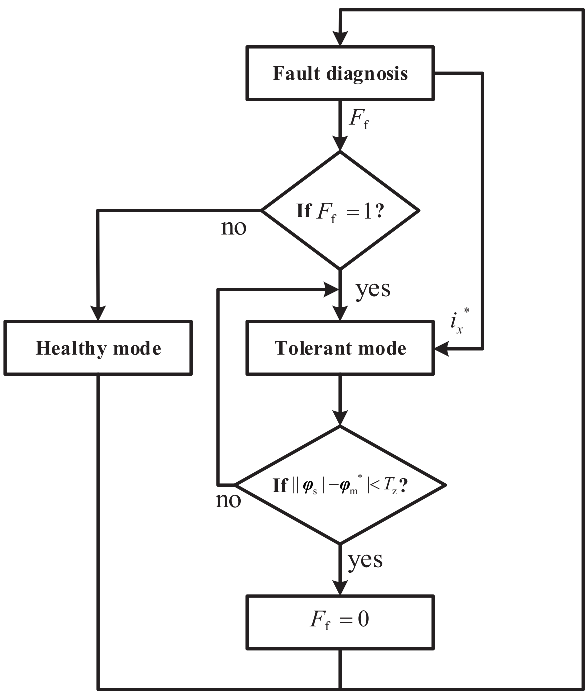

Fig. 5. The flow chart of control algorithm transition strategy.

value.

In actual application, the current protection must be considered. Meanwhile, the phase current of the fault leg should still be controlled to zero. Hence, when the phase current of the healthy leg is over the current limit, the fault phase component of v_s^* remains unchanged, and the healthy phase components of v_s^* are set to zero. The adjusted reference voltage vector is shown in Fig. 4. In Fig. 4, $\boldsymbol{v}_{s(a)}^*$, $\boldsymbol{v}_{s(b)}^*$, and $\boldsymbol{v}_{s(c)}^*$ represent the reference voltage vector. $\boldsymbol{v}_{s(a)}^*$, $\boldsymbol{v}_{s(b)}^*$, or $\boldsymbol{v}_{s(c)}^*$ is set to 0 under the fault conditions of inverter leg a, b, and c fault, respectively.

III. Control Algorithm Transition

Since the control algorithms under healthy and tolerant modes execute alternately in each current cycle, the smooth transition of control algorithms is one key point of the NFT.

In this paper, a control algorithm transition strategy is designed, which consists of the transition from healthy to tolerant mode and the transition from tolerant to healthy mode. Unlike the existing NFT methods, the fault switch is no longer seen as known. A MPFC-based fault diagnosis algorithm in our previous work [27] is used to realize the algorithm transition from healthy to tolerant mode for any switch fault. The deviation of the estimated stator flux amplitude and its reference value is used for the algorithm transition from tolerant to healthy mode. The flow chart is shown in Fig. 5, where F_f means the fault flag ('0' is healthy and '1' is faulty), and $\boldsymbol{i}_x^*$ means the reference value of fault phase current.

TABLE I
The Fault Diagnosis Lookup Table

F_a	F_b	F_c	F_f	i_x^*
$<-T_z$	$>T_z$	$>T_z$	1	$\boldsymbol{i}_a^*=0$
$>T_z$	$<-T_z$	$<-T_z$	1	$\boldsymbol{i}_a^*=0$
$>T_z$	$<-T_z$	$>T_z$	1	$\boldsymbol{i}_b^*=0$
$<-T_z$	$>T_z$	$<-T_z$	1	$\boldsymbol{i}_b^*=0$
$>T_z$	$>T_z$	$<-T_z$	1	$\boldsymbol{i}_c^*=0$
$<-T_z$	$<-T_z$	$>T_z$	1	$\boldsymbol{i}_c^*=0$

The fault diagnosis signals can be obtained by [27] as

$$\begin{bmatrix} F_a \\ F_b \\ F_c \end{bmatrix} = \begin{bmatrix} \boldsymbol{\varphi}_{sa}^k - \boldsymbol{\varphi}_{sa}^{*,k-1} \\ \boldsymbol{\varphi}_{sb}^k - \boldsymbol{\varphi}_{sb}^{*,k-1} \\ \boldsymbol{\varphi}_{sc}^k - \boldsymbol{\varphi}_{sc}^{*,k-1} \end{bmatrix} \tag{14}$$

where F_a, F_b, and F_c are three phase fault diagnosis signals. Then, F_f and $\boldsymbol{i}_x^*$ can be obtained by the fault diagnosis lookup table shown in Table I, where T_z is the fault diagnosis threshold value.

Since the above fault diagnosis is based on the error between the calculated $\boldsymbol{\varphi}_s^*$ and the actual $\boldsymbol{\varphi}_s$, the fault diagnosis will be disabled when the control algorithm of tolerant mode executes. It is because the error is slight under this algorithm. Hence, if no additional transition is used, the control algorithm of tolerant mode will always execute in the current cycle, wasting the healthy power switch.

Considering that the stator flux amplitude is constant in the control algorithm of healthy mode and variational in the tolerant mode, the transition can be smooth when they reach the same value. The judge of transition from tolerant to healthy mode can be expressed as

$$F_f = 0, \text{ if } ||\boldsymbol{\varphi}_s^*| - \boldsymbol{\varphi}_m^*| < T_z \tag{15}$$

Based on the combination of two transitions, even if there is a mistake in one transition, it can be corrected by another. This transition strategy has the ability to revert to healthy operation even if misdiagnoses occur. For example, when F_f is generated as '1', the control algorithm of tolerant mode is executed. After half the current cycle, it will automatically turn into the healthy mode with F_f as '0'. This process is repeated during each current cycle, which can greatly increase the reliability of the control algorithm transition.

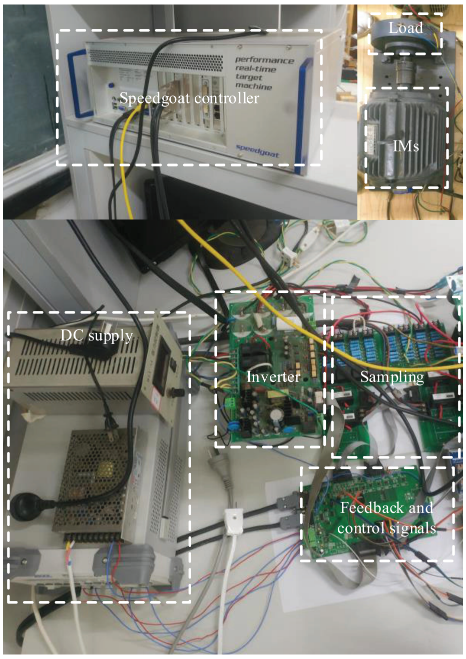

Fig. 6. The experimental platform.

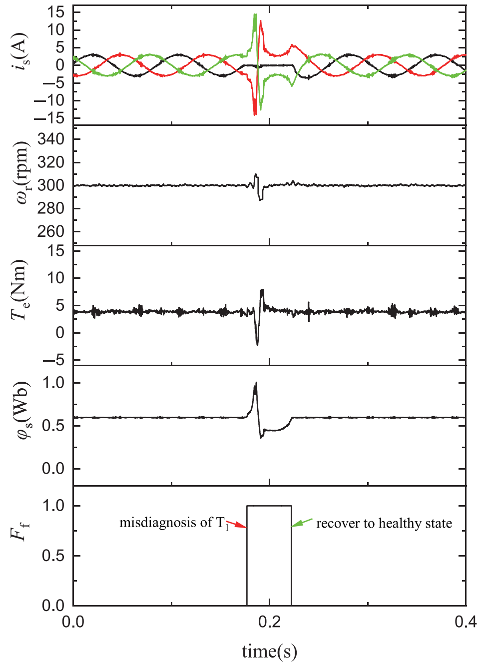

Fig. 7. The ability of anti-misdiagnosis of proposed NFT method.

TABLE II
PARAMETERS OF EXPERIMENTAL PLATFORM

Parameter	Value	Parameter	Value
DC-link voltage	400 V	Rotor inductance	330.03 mH
DC-link capacitor	2040 μF	Mutual inductance	319.7 mH
Sampling frequency	10 kHz	Rated power	2.2 kW
Dead time	2.5 μs	Rated speed	1430 r/min
Stator resistance	2.804 Ω	Rated current	4.9 A
Rotor resistance	2.178 Ω	Pole pairs	2
Stator inductance	330.03 mH	Rated Torque	10 Nm

IV. EXPERIMENTS

The experimental platform consists of a Speedgoat controller, one three-phase inverter (using IGBT PM25RSB120) with its power supply, sampling and control boards, and IM with magnetic powder brake, as Fig. 6 shows. The parameters of the experimental platform are presented in Table II.

Since the fault tolerance performances of six power switches are similar, T_1 fault is selected as the example to verify the effectiveness of the proposed method. The open-switch fault is simulated by putting the corresponding control signal as open. Fig. 7 presents the ability of anti-misdiagnosis of proposed NFT method. A misdiagnosis signal of T_1 is set at 0.19 s. It shows that even if misdiagnoses occur, the IM can automatically revert to the healthy operation state.

Fig. 8 presents the comparison of steady-state performance under the reference speed of 500 rpm and the load of 3 Nm. Here, the fault diagnosis threshold value T_z is set as a suitable value of 0.02. This value was determined through extensive experimental tests under various operating conditions (different speeds and loads) to ensure it was always greater than the maximum observed steady-state flux tracking error in healthy operation, thus preventing false alarms, while remaining small enough to enable rapid fault detection. The current limit value is set as 15 A to ensure safe operation. The reference value of stator flux amplitude is set as 0.6. The fault flag F_f shows the execution time of the control algorithms of healthy and tolerant modes. The speed oscillation is nearly 90 rpm (18% of reference speed) in Fig. 8(a). And the speed oscillation is nearly 40 rpm (8% of reference speed) in Fig. 8(b), which is nearly half of Fig. 8(a).

Fig. 9 presents the comparison of steady-state performance under the reference speed of 300 rpm and the load of 3 Nm. The speed oscillation is nearly 160 rpm (53.3% of reference speed) in Fig. 9(a). And the speed oscillation is reduced to nearly 25 rpm (8% of reference speed) in Fig. 9(b), which is much smoother than the former. It shows that when the reference speed is lower, the improvement of the proposed NFT method over fault operation is more significant.

Fig. 10 presents the comparison of steady-state performance under the reference speed of 500 rpm and the load of 7 Nm. The speed oscillation is nearly 220 rpm (44% of reference speed) in Fig. 10(a). And the speed oscillation is reduced to nearly 100 rpm (20% of reference speed) in Fig. 10(b). Compared to Fig. 8, the speed oscillations are increased because of the bigger load. The speed oscillation of proposed NFT method is still less than half of the case without tolerance.

Fig. 11 presents the speed-change performance under the reference speed of 300 to 500 rpm and the load of 3 Nm. Fig. 12 presents the load-change performance under the reference speed of 500 rpm and load of 3 to 7 Nm. It can be seen that the proposed NFT method is still effective during the dynamic process. Its response time is similar to the case without tolerance, and the dynamic response curve is much smoother.

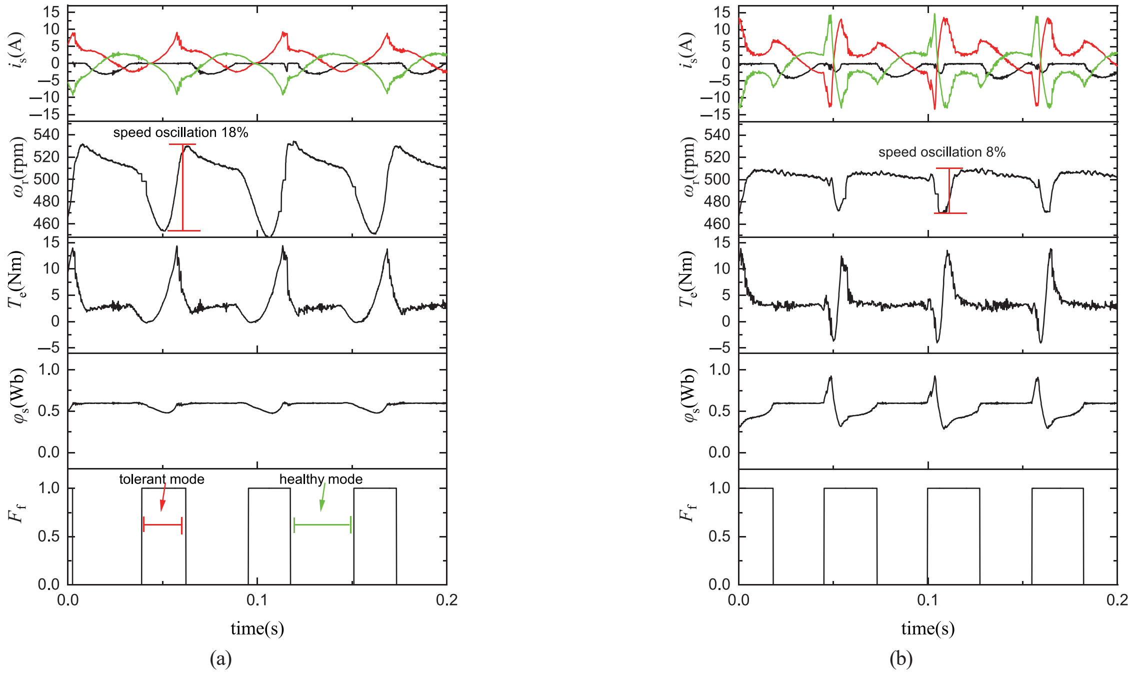

Fig. 8. The current, speed, torque, stator flux, and fault flag comparison of steady-state performance under the reference speed of 500 rpm and the load of 3 Nm: (a) without tolerance, (b) with proposed NFT method.

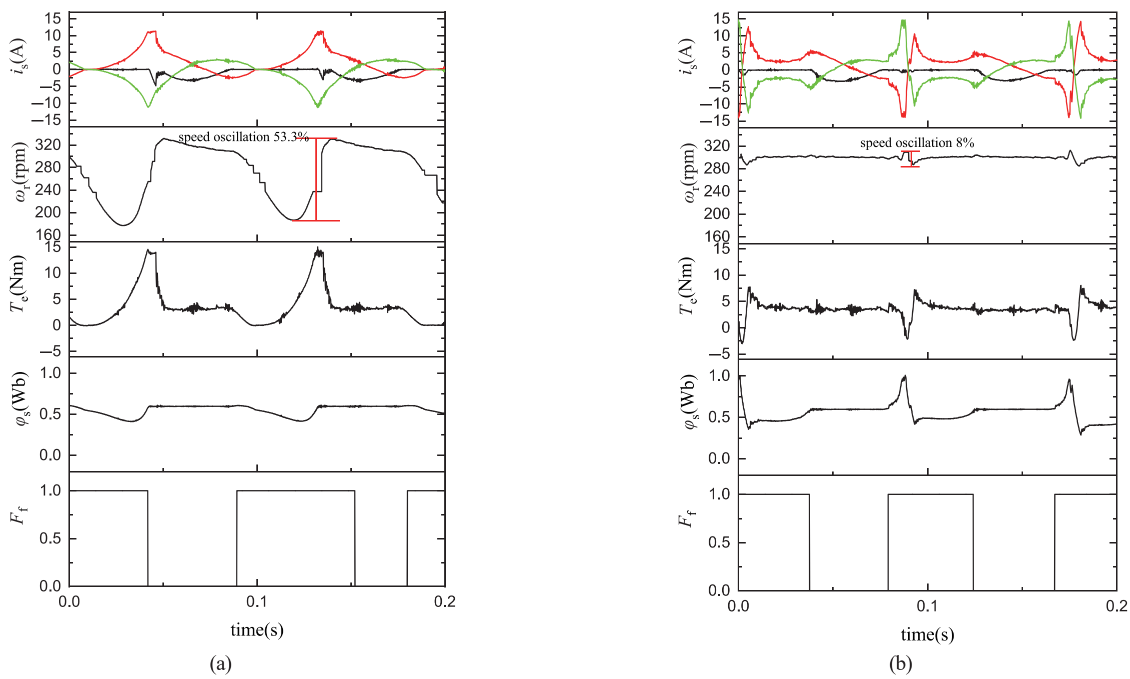

Fig. 9. The current, speed, torque, stator flux, and fault flag comparison of steady-state performance under the reference speed of 300 rpm and the load of 3 Nm: (a) without tolerance, (b) with proposed NFT method.

V. Compared with Other Methods

The proposed method is compared with other methods as shown in TABLE III. Traditional AFT methods often involve hardware reconfiguration (e.g., switching to a four-switch topology), which requires additional hardware (switches, relays) and complex control re-synthesis for each topology. In contrast, the proposed NFT method requires no hardware modification or reconfiguration, significantly reducing cost and complexity. The performance comparison is thus multifaceted: while some reconfiguration methods might achieve better post-fault performance theoretically, the proposed method offers a cost-to-performance ratio and simplicity of implementation, making it highly suitable for cost-sensitive applications where ultra-high post-fault performance is not the primary goal but continuous

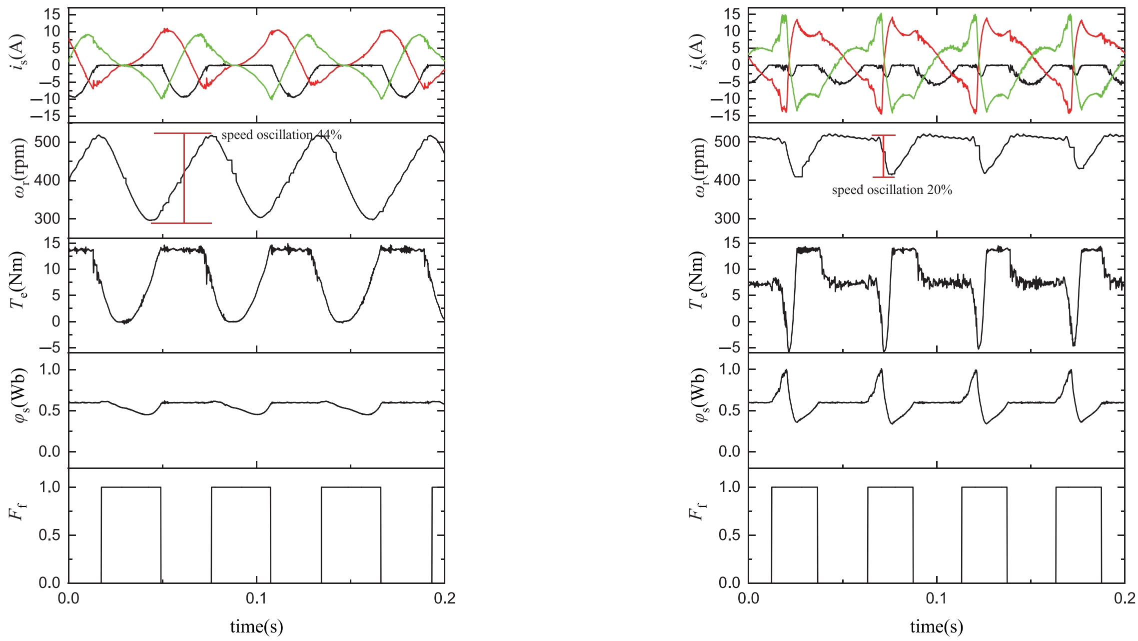

(a) (b)

Fig. 10. The current, speed, torque, stator flux, and fault flag comparison of steady-state performance under the reference speed of 500 rpm and the load of 7 Nm: (a) without tolerance, (b) with proposed NFT method.

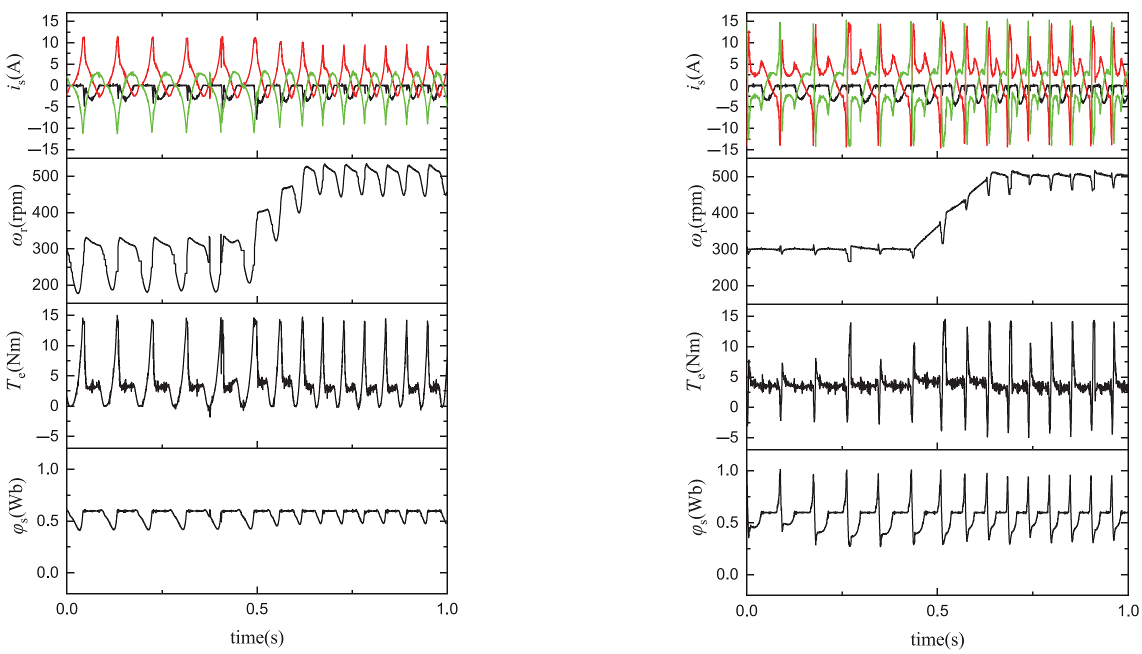

(a) (b)

Fig. 11. The current, speed, torque, and stator flux comparison of speed-change performance under the reference speed of 300 to 500 rpm and the load of 3 Nm: (a) without tolerance, (b) with proposed NFT method.

operation is. The experimental results provided demonstrate the significant performance gain over the non-tolerant case, which is the key benchmark for a fault-tolerant scheme.

The proposed method has the following advantages. Firstly, it avoids the transformation from a static to a rotating coordinate system and the estimation of electrical angles. Secondly, the existing methods all directly perform fault tolerance after obtaining the location of the power switch failure, without considering the impact of incorrect diagnosis. Once the fault diagnosis is incorrect, it will inevitably enter the fault-tolerant mode, wasting the power switches that are still healthy. However, the proposed method has the ability to automatically switch back to the healthy mode even if incorrect diagnosis occurs.

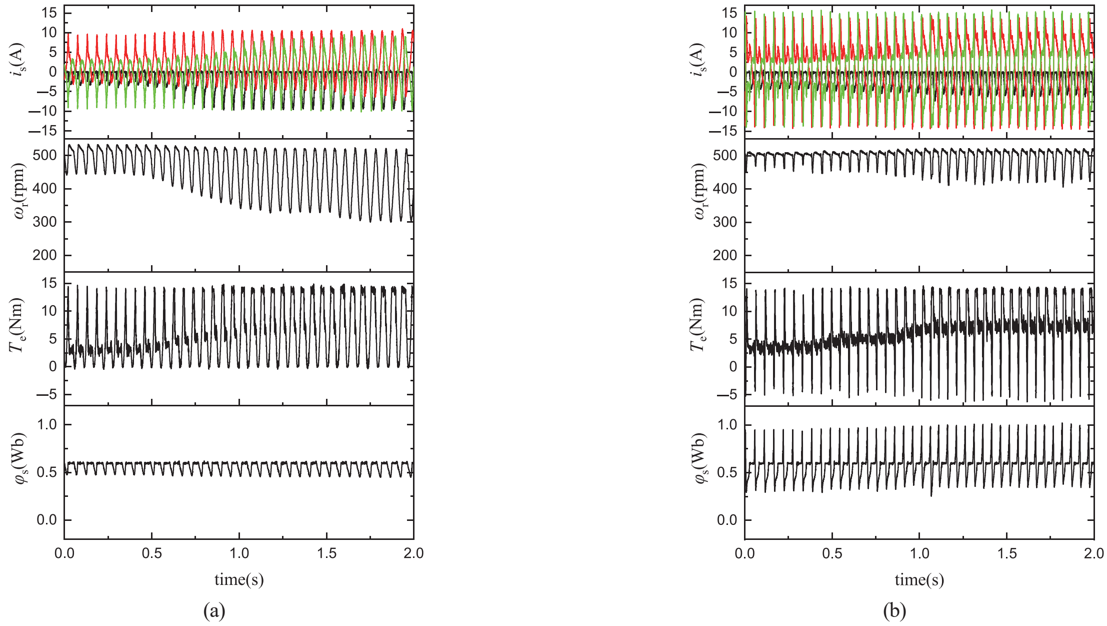

Fig. 12. The current, speed, torque, and stator flux comparison of load-change performance under the reference speed of 500 rpm and the load of 3 to 7 Nm: (a) without tolerance, (b) with proposed NFT method.

TABLE III
COMPARED WITH OTHER METHODS

Method	Topology	System signals needed	Transition stralegy	Fault location meeded	Hardwar /software cost	Remaining healthy switches utilixed
[3]	Four-leg inverter	Basic control signals	Recomstruction	Yes	High	No
[5]	Dual inverler	Basic control signals	Recomstruction	Yes	High	No
[7]	Multilevel inverter	Basic control signals	No-reconstruction	Yes	High	No
[11]	Four-switch inwerler	Basic control signals	Recomstruction	Yes	High	No
[14]	Four-switch four leg inverter	Basic control signals	Recomstruction	Yes	High	No
[24]	Basic tapology inwerler	Basic control signals Precise rodor angle estimation	No-reconstruction	Yes	Low	No
[26]	Basic tapology inwerler	Basic control signals Precise rodor angle estimation	No-reconstruction	Yes	Low	No
proposed	Basic tapology inwerler	Basic control signals	No-reconstruction srnouth trarsition	No	Low	Yes

VI. CONCLUSION

This paper proposes a novel no-reconstruction fault-tolerant method, which can realize the fault tolerance of standard IM drives without the requirement of topology reconstruction. Five healthy power switches are all used in fault tolerance. Thus, the system can work in the healthy state for half of each current cycle and in the tolerant state for the other half. Compared to existing NFT methods which also utilize five healthy power switches, the proposed method has the following contributions: first, the requirement of static-to-rotating coordinate transformation and electrical angle estimation is avoided based on the proposed two-mode control algorithm; second, a control algorithm transition strategy is designed, which can realize both the fast fault diagnosis and the smooth algorithm transition. Especially, it has the ability to revert to healthy operation even if misdiagnoses occur.

REFERENCES

[1] B. Lu and S. K. Sharma, “A literature review of IGBT fault diagnostic and protection methods for power inverters,” in *IEEE Transactions on Industry Applications*, vol. 45, no. 5, pp. 1770–1777, Sept.-Oct. 2009.

[2] W. Zhang, D. Xu, P. N. Enjeti, H. Li, J. T. Hawke, and H. S. Krishnamoorthy, “Survey on fault-tolerant techniques for power electronic converters,” in *IEEE Transactions on Power Electronics*, vol. 29, no. 12, pp. 6319–6331, Dec. 2014.

[3] R. R. Errabelli and P. Mutschler, “Fault-tolerant voltage source inverter for permanent magnet drives,” in *IEEE Transactions on Power Electronics*, vol. 27, no. 2, pp. 500–508, Feb. 2012.

[4] P. Garg, S. Essakiappan, H. S. Krishnamoorthy, and P. N. Enjeti, “A fault-tolerant three-phase adjustable speed drive topology with active common-mode voltage suppression,” in *IEEE Transactions on Power Electronics*, vol. 30, no. 5, pp. 2828–2839, May 2015.

[5] Z. Wang, J. Chen, M. Cheng, and Y. Zheng, “Fault-tolerant control of paralleled-voltage-source-inverter-fed PMSM drives,” in *IEEE Transactions on Industrial Electronics*, vol. 62, no. 8, pp. 4749–4760, Aug. 2015.

[6] G. Chen and X. Cai, "Reconfigurable control for fault-tolerant of parallel converters in PMSG wind energy conversion system," in *IEEE Transactions on Sustainable Energy*, vol. 10, no. 2, pp. 604–614, Apr. 2019.

[7] X. Wang, Z. Wang, Z. Xu, J. He, and W. Zhao, "Diagnosis and tolerance of common electrical faults in T-type three-level inverters fed dual three-phase PMSM drives," in *IEEE Transactions on Power Electronics*, vol. 35, no. 2, pp. 1753–1769, Feb. 2020.

[8] X. Wang, Z. Wang, M. Gu, Z. Xu, Z. Zou, W. Wang, and M. Cheng, "Fault-tolerant control of common electrical faults in dual three-phase PMSM drives fed by T-type three-level inverters," in *IEEE Transactions on Industry Applications*, vol. 57, no. 1, pp. 481–491, Jan.-Feb. 2021.

[9] W. Huang, J. Du, W. Hua, W. Lu, K. Bi, Y. Zhu, and Q. Fan, "Current-based open-circuit fault diagnosis for PMSM drives with model predictive control," in *IEEE Transactions on Power Electronics*, vol. 36, no. 9, pp. 10695–10704, Sept. 2021.

[10] X. Zhou, J. Sun, P. Cui, Y. Lu, M. Lu, and Y. Yu, "A fast and robust open-switch fault diagnosis method for variable-speed PMSM system," in *IEEE Transactions on Power Electronics*, vol. 36, no. 3, pp. 2598–2610, Mar. 2021.

[11] M. Tousizadeh, H. S. Che, J. Selvaraj, N. A. Rahim, and B. -T. Ooi, "Fault-tolerant field-oriented control of three-phase induction motor based on unified feedforward method," in *IEEE Transactions on Power Electronics*, vol. 34, no. 8, pp. 7172–7183, Aug. 2019.

[12] D. Sun, J. Su, C. Sun, and H. Nian, "A simplified MPFC with capacitor voltage offset suppression for the four-switch three-phase inverter-fed PMSM drive," in *IEEE Transactions on Industrial Electronics*, vol. 66, no. 10, pp. 7633–7642, Oct. 2019.

[13] K. Hu, Z. Liu, I. A. Tasiu, and T. Chen, "Fault diagnosis and tolerance with low torque ripple for open-switch fault of IM drives," in *IEEE Transactions on Transportation Electrification*, vol. 7, no. 1, pp. 133–146, Mar. 2021.

[14] W. Li, S. Xuan, Q. Gao, and L. Luo, "Investigation of a four-switch four-leg inverter: Modulation, control, and application to an IPMSM drive," in *IEEE Transactions on Power Electronics*, vol. 34, no. 6, pp. 5655–5666, Jun. 2019.

[15] T. Liu and M. Fadel, "An efficiency-optimal control method for mono-inverter dual-PMSM systems," in *IEEE Transactions on Industry Applications*, vol. 54, no. 2, pp. 1737–1745, Mar.-Apr. 2018.

[16] T. Liu, M. Fadel, J. Li, and X. Ma, "A MTPA control strategy for mono-inverter multi-PMSM system," in *IEEE Transactions on Power Electronics*, vol. 36, no. 6, pp. 7165–7177, Jun. 2021.

[17] Š. Janouš, J. Talla, V. Šmídl, and Z. Peroutka, "Constrained LQR control of dual induction motor single inverter drive," in *IEEE Transactions on Industrial Electronics*, vol. 68, no. 7, pp. 5548–5558, Jul. 2021.

[18] S. Ito, T. Moroi, Y. Kubo, K. Matsuse, and K. Rajashekara, "Independent control of two permanent-magnet synchronous motors fed by a four-leg inverter," in *IEEE Transactions on Industry Applications*, vol. 51, no. 1, pp. 753–760, Jan.-Feb. 2015.

[19] Y. Song, J. Sun, Y. Zhou, Y. Liu, H. Luo, and J. Zhao, "Minimization of capacitor voltage difference for four-leg inverter dual-parallel IM system," in *IEEE Transactions on Power Electronics*, vol. 37, no. 4, pp. 3969–3979, Apr. 2022.

[20] W. Wang, J. Zhang, and M. Cheng, "A dual-level hysteresis current control for one five-leg VSI to control two PMSMs," in *IEEE Transactions on Power Electronics*, vol. 32, no. 1, pp. 804–814, Jan. 2017.

[21] Y. -S. Lim, J. -S. Lee, and K. -B. Lee, "Advanced speed control for a five-leg inverter driving a dual-induction motor system," in *IEEE Transactions on Industrial Electronics*, vol. 66, no. 1, pp. 707–716, Jan. 2019.

[22] A. Kontarček, P. Bajec, M. Nemec, V. Ambrožič, and D. Nedeljković, "Cost-effective three-phase PMSM drive tolerant to open-phase fault," in *IEEE Transactions on Industrial Electronics*, vol. 62, no. 11, pp. 6708–6718.

[23] M. Moujahed, M. Hajji, H. Benazza, M. Jemli, and M. Boussak, "Fault tolerant control of permanent magnet synchronous motor traction module," *2018 9th International Renewable Energy Congress (IREC)*, Hammamet, Tunisia, 2018, pp. 1–5.

[24] C. M. Hackl, U. Pecha, and K. Schechner, "Modeling and control of permanent-magnet synchronous generators under open-switch converter faults," in *IEEE Transactions on Power Electronics*, vol. 34, no. 3, pp. 2966–2979, Mar. 2019.

[25] X. Wang, Z. Wang, M. Gu, B. Wang, W. Wang, and M. Cheng, "Current optimization-based fault-tolerant control of standard three-phase PMSM drives," in *IEEE Transactions on Energy Conversion*, vol. 36, no. 2, pp. 1023–1035, Jun. 2021.

[26] Z. Zhang, Y. Hu, G. Luo, C. Gong, X. Liu, and S. Chen, "An embedded fault-tolerant control method for single open-switch faults in standard PMSM drives," in *IEEE Transactions on Power Electronics*, vol. 37, no. 7, pp. 8476–8487, Jul. 2022.

[27] Y. Song and J. Zhao, "Model predictive flux control-based open-circuit fault diagnosis method for two-level three-phase inverter induction motor drive," in *2022 41st Chinese Control Conference (CCC)*, Hefei, China, 2022, pp. 3912–3916.

Lei Wang was born in January 1982. He graduated from Huazhong University of Science and Technology with the master's degree. Currently, he is a senior engineer at Wuhan Second Ship Design and Research Institute. He has been engaged in the research of ship electrical systems and equipment for a long time, and has been responsible for the research and equipment development of multiple ship electrical devices.

Yingying She was born in November 1983. She obtained her doctoral degree from Huazhong University of Science and Technology. Currently, she is a researcher at Wuhan Second Ship Design and Research Institute. She has been engaged in the research and development of ship control systems for a long time and has undertaken the overall design of various ship electrical and control systems.

Yujin Song was born in Heilongjiang, China, in 1996. He received the B.S. degree and the Ph.D. degree in Control Science and Engineering, in 2017 and 2023, from the Department of Control Science and Engineering, School of Automation, Huazhong University of Science and Technology, Wuhan, China. Currently, he is working at Wuhan Second Ship Design and Research Institute. His research interests include fault tolerant control and advanced control strategies for power electronics and power converter.

Weikang Wang was born in Hubei Province, China, in 1996. He received the B.S. degree and the Ph.D. degree in 2017 and 2023 from the School of Automation, Huazhong University of Science and Technology, Wuhan, China. Currently, he is working at Wuhan Second Ship Design and Research Institute. His research interests include DC–DC converters and high frequency power conversion.

Zhixi Wu was born in Henan, China, in 1996. He received the B.S. degree in Automation from Hunan University, Changsha, China, in 2018, as well as the M.S. degree and the Ph.D. degree in control science and engineering from the Huazhong University of Science and Technology, Wuhan, China, in 2021 and 2025. Currently, he is working at Wuhan Second Ship Design and Research Institute. His research interests include multilevel converters and fault diagnosis for power converters.